Supplemental material

Nakajima et al., https://doi.org/10.1083/jcb.201803116

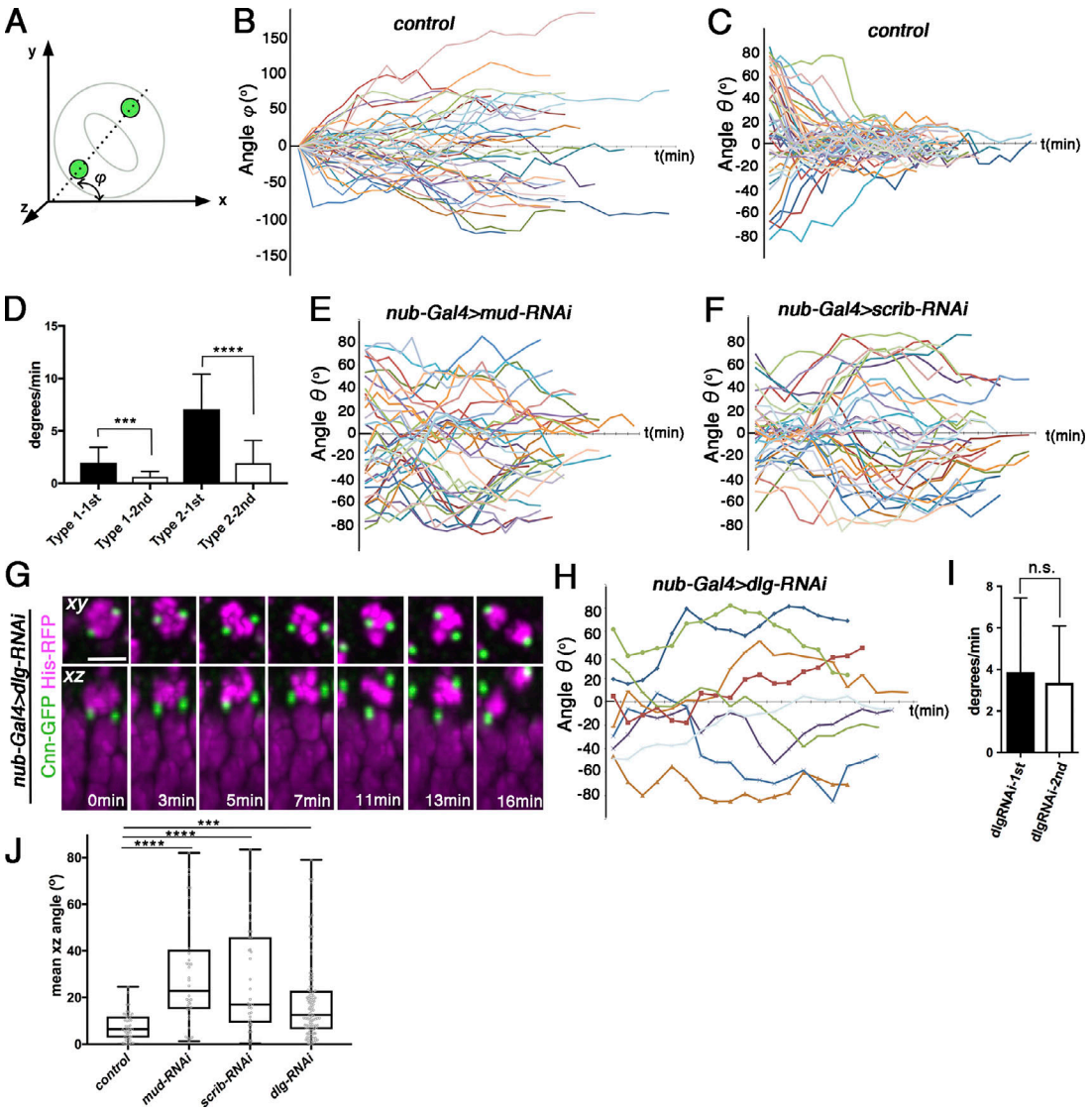

Figure S1. **Mitotic spindle movements during planar orientation and randomized movements in Mud-, Scrib-, and Dlg-depleted cells. (A)** To quantify mitotic spindle orientation within the epithelial plane, ϕ represents the angle in *xy* plane between the spindle axis (line through spindle poles) and the x axis. **(B)** *Xy* rotation dynamics during prometaphase and metaphase for control dividing cells (*n* = 45). Each color curve represents an individual mitotic cell. **(C)** *Z* rotation dynamics during prometaphase and metaphase for control dividing cells (*n* = 45). **(D)** The relative *z* rotation speed for type 1 (*n* = 19) and type 2 (*n* = 26) control dividing cells. The *z* rotations were measured during the first and second halves of orientation. Error bars are SD. ****, P < 0.0001; ***, P = 0.0002 (paired two-tailed *t* test). **(E and F)** *Z* rotation dynamics during prometaphase and metaphase for *mud-RNAi* (n = 36; E) or *scrib-RNAi* (*n* = 35; F) dividing cells. **(G)** Time-lapse series of mitotic wing disc cells exhibiting aberrant anaphase spindle orientation for *dlg-RNAi*. **(H)** *Z* rotation dynamics during prometaphase and metaphase for *dlg-RNAi*. Each color curve represents individual mitotic cell (nine representative cells are shown from *dlg-RNAi*, *n* = 102). **(I)** The relative z rotation speed for *dlg-RNAi*. The expected z rotation-speed reduction between the first and second halves (see Fig. 1 E) diminished in *dlg-RNAi* cells (*n* = 102). Error bars are SD. n.s., not significant (P > 0.05) by paired two-tailed *t* test. **(J)** The distribution of anaphase-telophase spindle angles from time-lapse data for different RNAi wing discs. Data are shown as box plots (median ± quartiles). Each point represents a cell. Control, *n* = 44; *mud-RNAi*, *n* = 36; *scrib-RNAi*, *n* = 35; *dlg-RNAi*, *n* = 102. ****, P < 0.0001; ***, P = 0.0001 by Kolmogorov–Smirnov test. Scale bar in G: 5 µm.

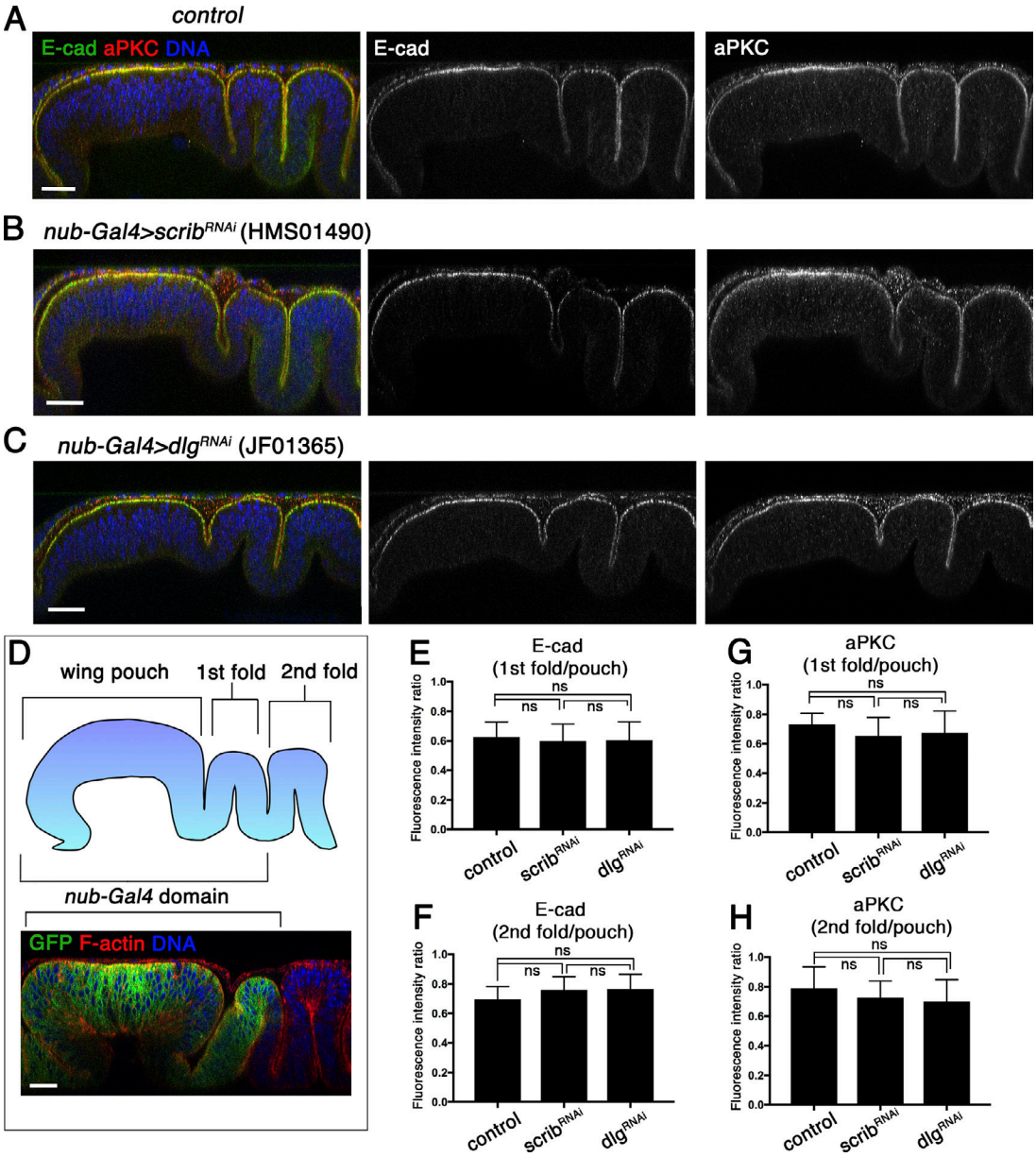

Figure S2. **Apico-basal polarity is maintained in *scrib-RNAi* or *dlg-RNAi* wing discs. (A–C)** Optical cross sections immunostained for adherens junction (E-cadherin [E-cad]) and apical polarity (aPKC) markers in control (*nub-Gal4/+*; A), *scrib*-knockdown (*nub-Gal4>scrib-RNAi*, HMS01490; B), and *dlg*-knockdown (*nub-Gal4>dlg-RNAi*, JF01365; C). **(D)** Schematic illustration of the wing disc structure and a representative image of the *nub-Gal4>mCD8-GFP* wing disc. *nub-Gal4* is expressed in both the wing pouch and the first fold, not in the second fold. Scale bars in A–D: 20 µm. **(E–H)** Quantification for fluorescent intensity of E-cadherin in the first fold (E) and the second fold (F), as well as aPKC in the first fold (G) and the second fold (H). Fluorescent intensity in each fold region is normalized by dividing with the intensity in the wing pouch. The number of samples are as follows: control, *n* = 20; *scrib-RNAi*, *n* = 20; *dlg-RNAi*, *n* = 14. Error bars are SD. n.s., not significant (P > 0.05) by one-way ANOVA with multiple comparison test.

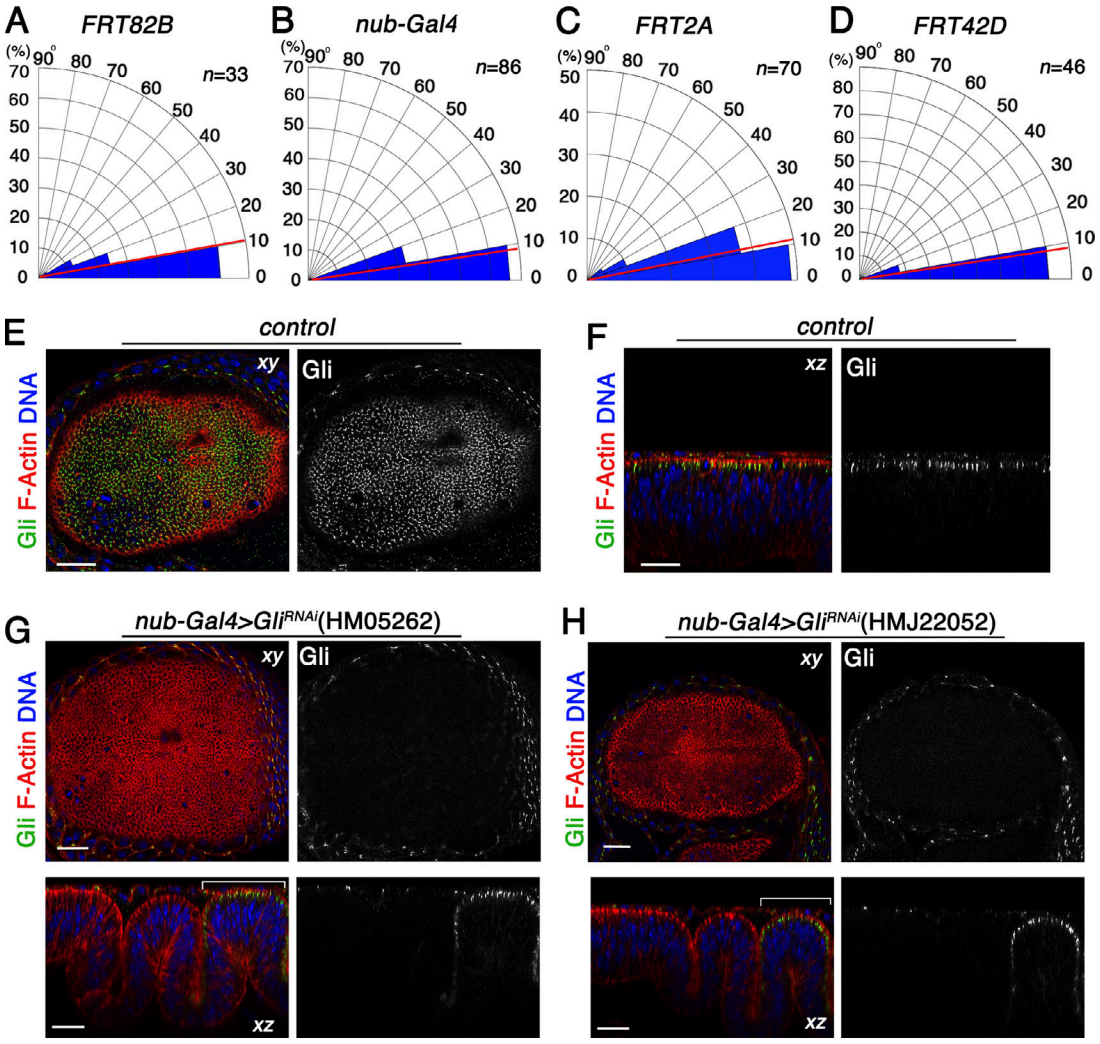

Figure S3. **Spindle orientation in controls and validation of *Gli*-RNAi constructs. (A–D)** Quantification of mitotic spindle alignments in *FRT82B* (A), *nub-Gal4* (B), *FRT2A* (C), and *FRT42D* (D) controls. The red lines show the median angular deviation. *n* indicates the number of spindles observed. **(E and F)** Control wing disc stained with anti-Gli in *xy* (E) and *xz* (F) images. **(G and H)** *Gli*-knockdown wing discs (*nub-Gal4>Gli-RNAi*) stained with anti-Gli. Two different constructs for *Gli*-RNAi, HM05262 (G) and HMJ22052 (H) were expressed, respectively, under the *nub-Gal4* driver. Brackets show the region where *nub-Gal4* is not expressed. Scale bars in E–H: 20 µm.

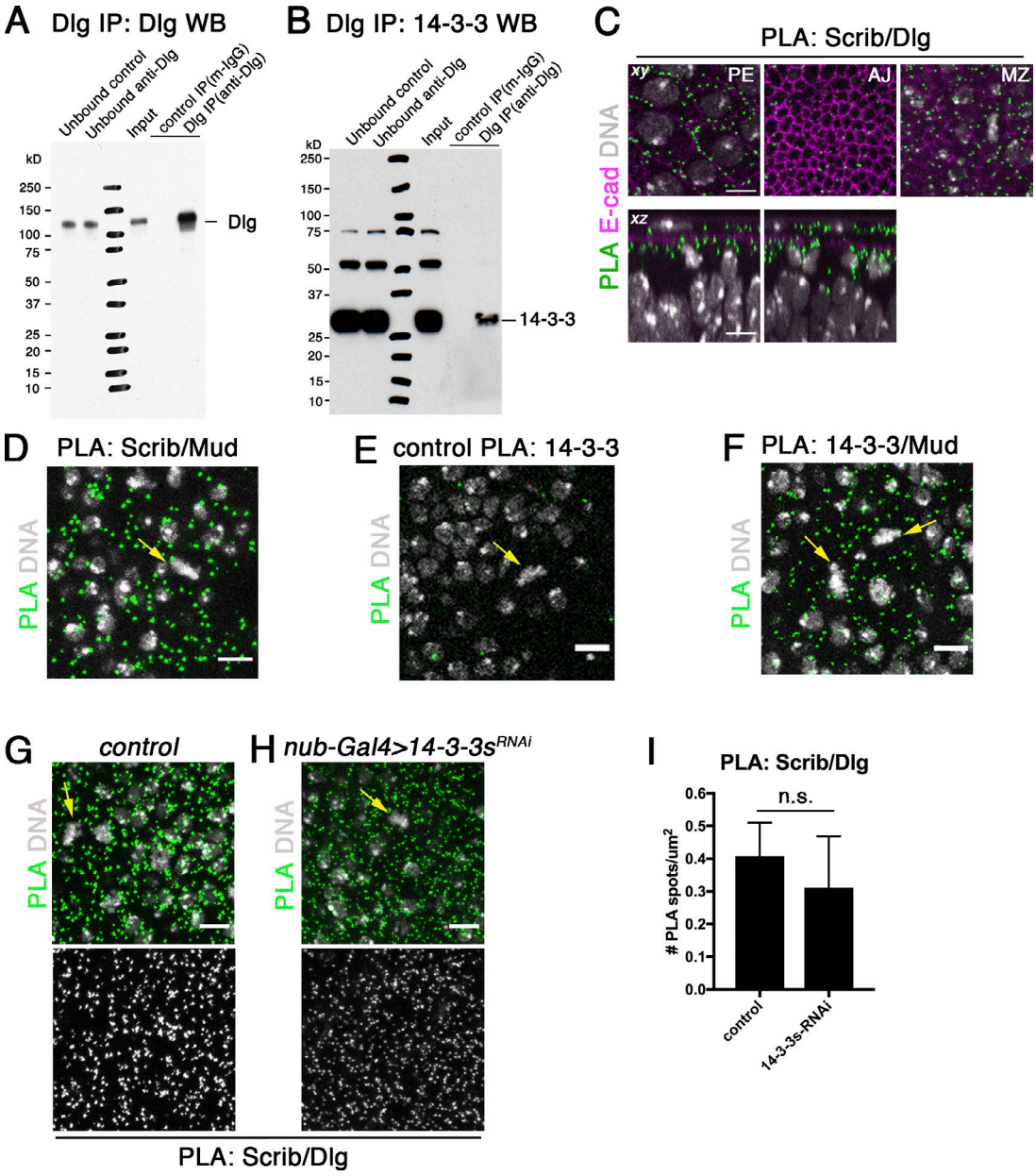

Figure S4. **Original Western blot for immunoprecipitation/coimmunoprecipitation and in situ PLA among Dlg, Scrib, 14-3-3, and Mud. (A and B)** Original Western blot images for Dlg immunoprecipitation (IP; A) and coimmunoprecipitation of Dlg and 14-3-3 (Dlg IP with 14-3-3 Western blot [WB]; B). **(C)** PLA between Scrib and Dlg in wild-type wing discs stained with anti–E-cadherin. PLA spots were located to the junctional region of peripodial epithelium (PE) and to the mitotic zone (MZ) of the disc proper, which is below the adherens junctions (AJ). **(D–F)** PLA between Scrib and Mud (D), control PLA using only anti–14-3-3 antibody (E), and PLA between 14-3-3 and Mud (F) in wild-type wing discs. **(G and H)** PLA between Scrib and Dlg in control (G) and *14-3-3s* knockdown (H). **(I)** Quantification of the number of PLA (Scrib/Dlg) spots for control (n = 6) and *14-3-3s-RNAi* (n = 5) wing discs. n.s., not significant ($P > 0.05$) by Kolmogorov–Smirnov test. Yellow arrows indicate metaphase cells. n.s., not significant. Scale bars: 5 µm.

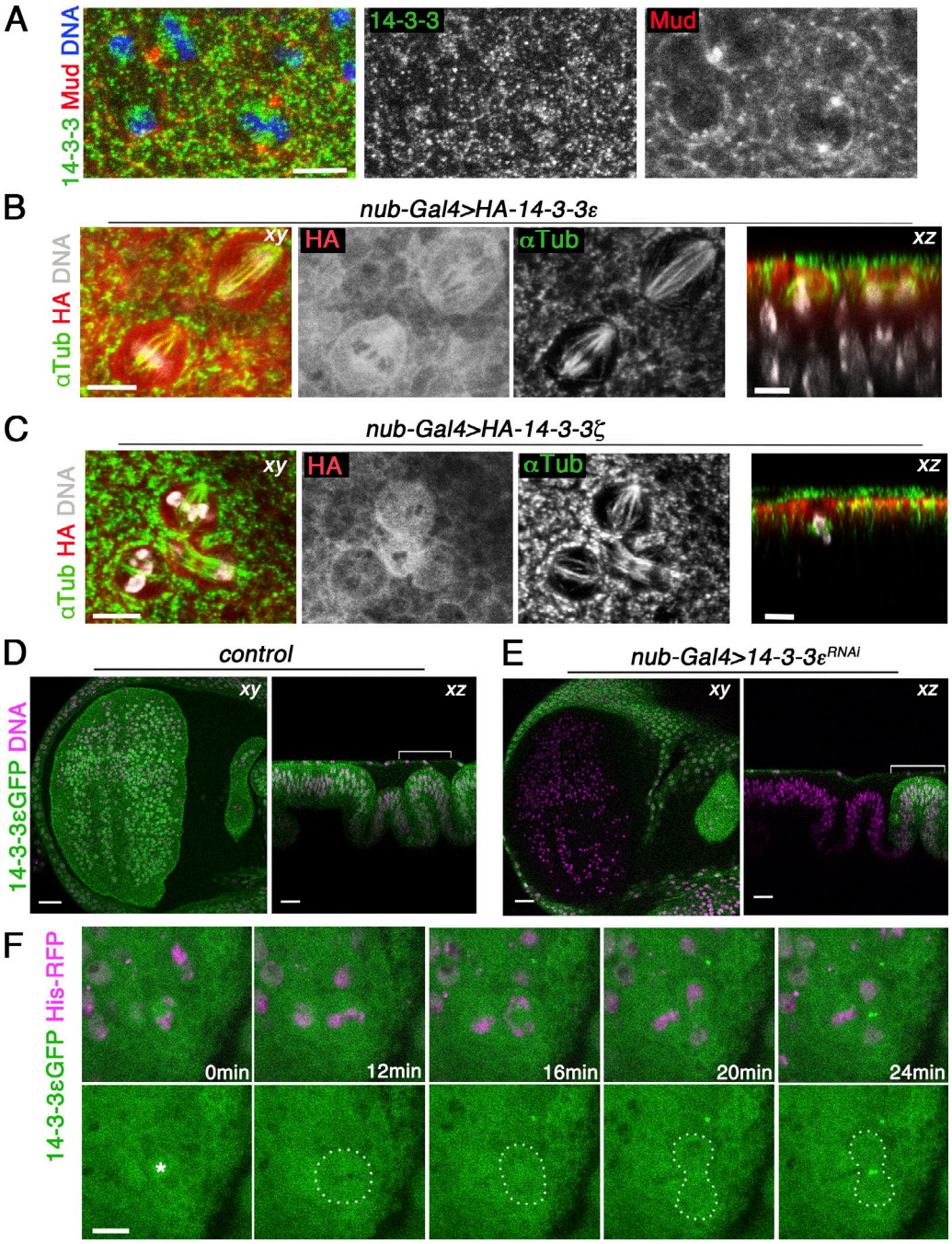

Figure S5. **Subcellular localization of 14-3-3 proteins during mitosis. (A)** Subcellular localization of 14-3-3 proteins and Mud detected by anti–14-3-3 antibody and anti-Mud antibody, respectively. **(B and C)** Subcellular localization of HA-tagged 14-3-3 proteins detected by anti-HA antibody staining. HA-tagged 14-3-3 proteins localize to the apical cortex in interphase and cytosol including spindle microtubules (α-tubulin) during mitosis. *HA-14-3-3ε or HA-14-3-3ζ* is expressed in the wing pouch driver (*nub-Gal4>HA-14-3-3ε*, B; *nub-Gal4>HA-14-3-3ζ*, C). **(D and E)** Fixed images of wing disc cells expressing 14-3-3ε-GFP in control (*nub-Gal4/+*; D) and *14-3-3ε*-knockdown (*nub-Gal4>14-3-3ε-RNAi*, HMS01229; E). Brackets show the region where *nub-Gal4* is not expressed. **(F)** Time-lapse images of dividing wing disc cells expressing 14-3-3ε-GFP (green) and His2Av-mRFP (His-RFP; magenta). 14-3-3ε-GFP exhibits enrichment at the apical cortex during interphase followed by a cytosolic redistribution during mitosis and a strong concentration in the midbody during cytokinesis. An asterisk (0 min) indicates the cell that enters mitosis (outlined by dotted lines). Scale bars: 5 µm.

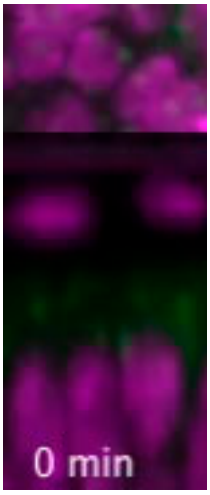

Video 1. **Representative time-lapse video of type 1 dividing cells in control wing discs.** The xy projection of z stacks (upper panels) and vertical xz sections (lower panels). Cnn-GFP, green; His2Av-mRFP, magenta. Frames were taken every 1 min.

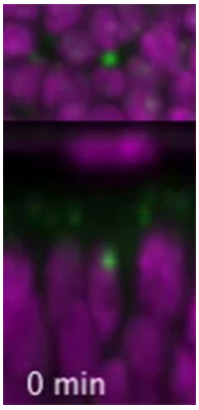

Video 2. **Representative time-lapse video of type 2 dividing cells in control wing discs.** The xy projection of z stacks (upper panels) and vertical xz sections (lower panels). Cnn-GFP, green; His2Av-mRFP, magenta. Frames were taken every 1 min.

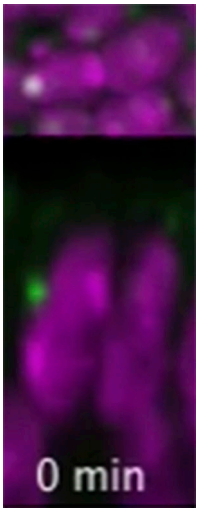

Video 3. **Representative time-lapse video of mitotic wing disc cells exhibiting aberrant spindle orientation for*mud-RNAi.*** The xy projection of z stacks (upper panels) and vertical xz sections (lower panels). Cnn-GFP, green; His2Av-mRFP, magenta. Frames were taken every 1 min.

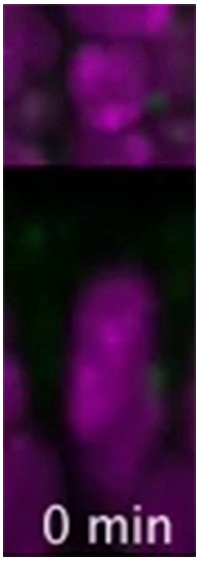

Video 4. **Representative time-lapse video of mitotic wing disc cells exhibiting aberrant spindle orientation for*scrib-RNAi.*** The xy projection of z stacks (upper panels) and vertical xz sections (lower panels). Cnn-GFP, green; His2Av-mRFP, magenta. Frames were taken every 1 min.

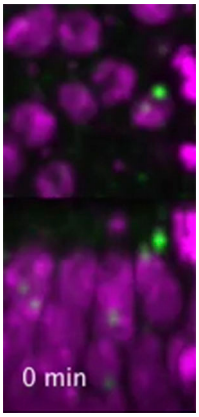

Video 5. **Representative time-lapse video of mitotic wing disc cells exhibiting aberrant spindle orientation for*dlg-RNAi.*** The xy projection of z stacks (upper panels) and vertical xz sections (lower panels). Cnn-GFP, green; His2Av-mRFP, magenta. Frames were taken every 1 min.

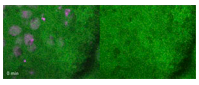

Video 6. **Time-lapse imaging of dividing wing disc cells expressing *14-3-3ε-GFP*.** Merged images (left panels) and GFP-only images (right panels). 14-3-3ε-GFP, green; His2Av-mRFP, magenta. Frames were taken every 2 min.

Provided online is one table in Excel. Table S1 shows proteins copurified with Dlg or Scrib, immunoprecipitated from fly embryos, and analyzed by MudPIT.